Type I Collagen *D*-Spacing in Fibril Bundles of Dermis, Tendon, and Bone: Bridging between Nano- and Micro-Level Tissue Hierarchy

Ming Fang,[†,‡] Elizabeth L. Goldstein,[†] A. Simon Turner,[▲] Clifford M. Les,[△] Bradford G. Orr,[‡,§,⊥] Gary J. Fisher,[∥] Kathleen B. Welch,[¶] Edward D. Rothman,[¶,#] and Mark M. Banaszak Holl[†,‡,⊥,*]

[†]Department of Chemistry, [‡]Michigan Nanotechnology Institute for Medicine and Biological Science, [§]Department of Physics, [⊥]Program in Applied Physics, [∥]Department, of Dermatology, [¶]Center for Statistical Consultation and Research, [#]Department of Statistics, University of Michigan, Ann Arbor, Michigan 48109, United States, [△]Bone and Joint Center, Henry Ford Hospital, Detroit, Michigan 48202, United States, and [▲]College of Veterinary Medicine & Biomedical Sciences, Colorado State University, Fort Collins, Colorado 80309, United States

ABSTRACT Fibrillar collagens in connective tissues are organized into complex and diverse hierarchical networks. In dermis, bone, and tendon, one common phenomenon at the micrometer scale is the organization of fibrils into bundles. Previously, we have reported that collagen fibrils in these tissues exhibit a 10 nm width distribution of *D*-spacing values. This study expands the observation to a higher hierarchical level by examining fibril *D*-spacing distribution in relation to the bundle organization. We used atomic force microscopy imaging and two-dimensional fast Fourier transform analysis to investigate dermis, tendon, and bone tissues. We found that, in each tissue type, collagen fibril *D*-spacings within a single bundle were nearly identical and frequently differ by less than 1 nm. The full 10 nm range in *D*-spacing values arises from different values found in different bundles. The similarity in *D*-spacing was observed to persist for up to 40 μm in bundle length and width. A nested mixed model analysis of variance examining 107 bundles and 1710 fibrils from dermis, tendon, and bone indicated that fibril *D*-spacing differences arise primarily at the bundle level (~76%), independent of species or tissue types.

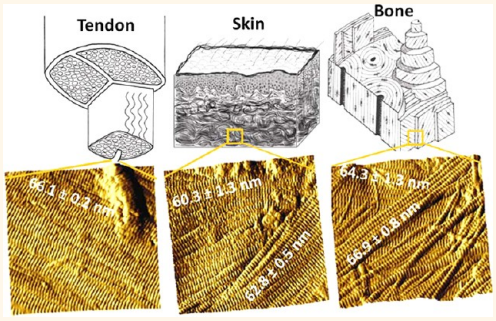

KEYWORDS: collagen bundle · fibril *D*-spacing · AFM · 2D FFT · mixed model ANOVA

Noncartilaginous connective tissues, including dermis, tendon, and bone, are predominantly composed of type I fibrillar collagen in the organic phase of their extracellular matrix (ECM). As the main ECM building block, collagen fibrils play pivotal roles in maintaining tissue integrity, providing the basis for mechanical properties and influencing cell activities. Collagen fibrils have an exceptionally long half-life *in vivo*, which is estimated to be 15−95 years.[1,2] They are resistant to common proteases since the tightly packed fibrillar structure prevents access to cleavage sites.[3] Collagen fibrils are mechanically tough;[4] as a structural network, they enhance cell attachment, migration, and differentiation.[5,6]

The properties of ECM derive in part from the hierarchical structure of collagen molecules, fibrils, fibril bundles, and higher levels of organization (Figure 1). The fibril-forming collagen molecules (types I, III, V, XI, *etc.*) share similar structural motifs. Each of the three α-helices contains Gly-X-Y repeating triplets, with proline and hydroxyproline being the most common X and Y residues.[7] The molecular packing of collagen fibril was studied by X-ray in the 1960s to 1980s.[8−15] The fibrils are composed of five-stranded microfibrils that are quasi-hexagonally packed in the equatorial plane[8,9,12−14,16] and supertwisted in the axial direction.[3] Within a fibril, as the Hodge−Petruska model depicts, collagen molecules are aligned in a parallel staggered manner giving a repeating gap/overlap pattern, resulting in the observed *D*-spacing.[3,17]

The next level of collagen hierarchy in ECM is the organization of fibrils into bundles, which occurs at micrometer to millimeter scale (Figure 1). Qualitatively, a bundle is a group of parallel fibrils that are generally associated with each other *via* interfibrillar cross-links.[18] In dermis and tendon, a bundle is frequently referred to as a fiber, whereas in bone, it is a lamella sheet of

* Address correspondence to mbanasza@umich.edu.

Received for review June 5, 2012 and accepted October 2, 2012.

Published online October 22, 2012
10.1021/nn302483x

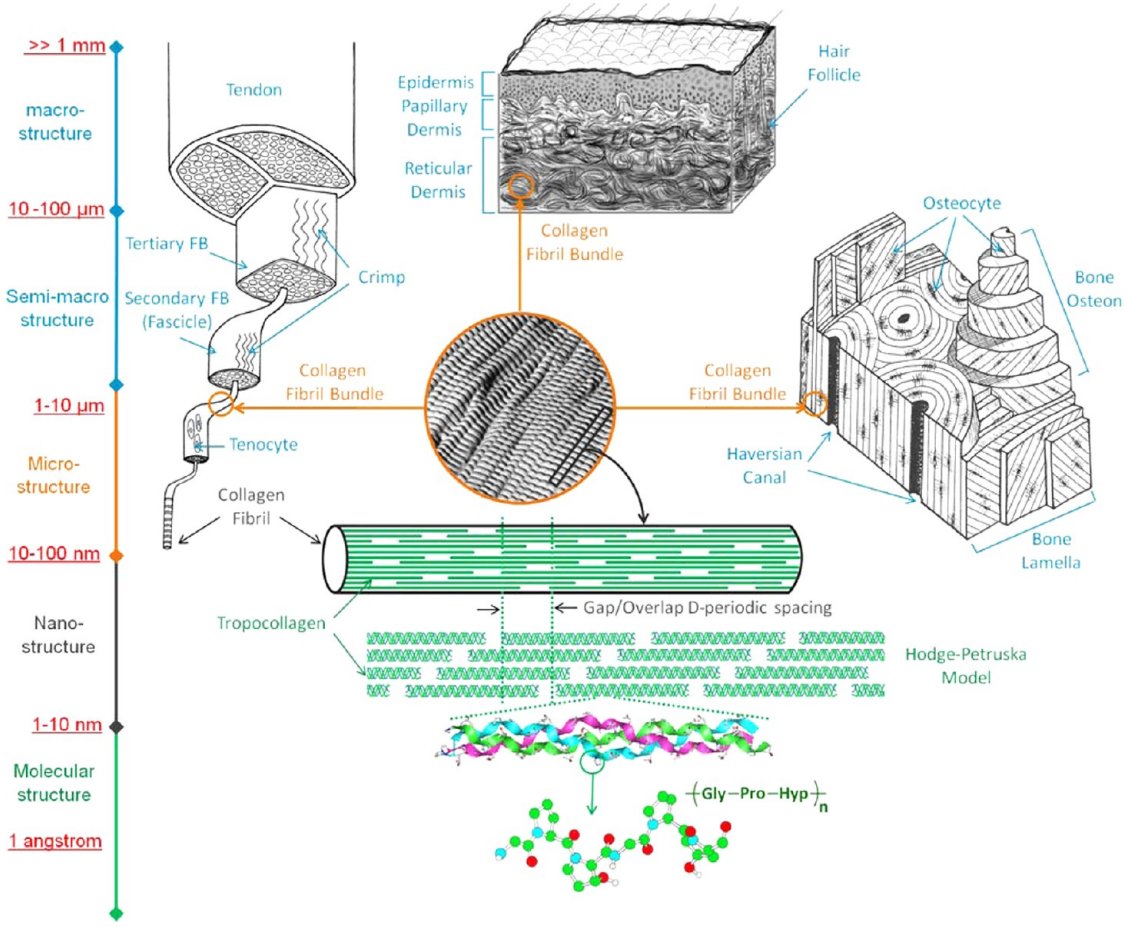

Figure 1. Schematic representations of hierarchical tissue structures of tendon, skin, and bone. FB is short for fiber bundle.

parallel collagen fibrils. The micrometer-scale organization of fibril bundles varies dramatically among tissues. As shown in Figure 1, in the dermis, bundles of collagen fibrils with a lateral size ranging from tens of micrometers to a few hundred micrometers are randomly oriented in a three-dimensional meshwork.[19,20] Tendon has an overall uniaxial structure where collagen fibrils are aligned in parallel arrays.[21,22] Bone adapts a twisted plywood structure constructed by lamellae of collagen fibrils with alternating fibril angles among different lamella sheets.[23−25] Despite the significantly different ECM organizations described above, the grouping of collagen fibrils into micrometer-scale bundles is ubiquitous among collagenous tissues.[26−28]

Characterization of fibril bundles in connective tissues has been limited to qualitative descriptions. For example, scanning electron microscopy (SEM), transmission electron microscopy (TEM), and circularly polarized light microscopy imaging have been used for visualization of dermal fibril bundles and bone lamellae.[19,24,29,30] We have recently developed a quantitative method for *D*-spacing analysis at the micrometer to submicrometer scale, using atomic force microscopy (AFM) imaging and two-dimensional fast

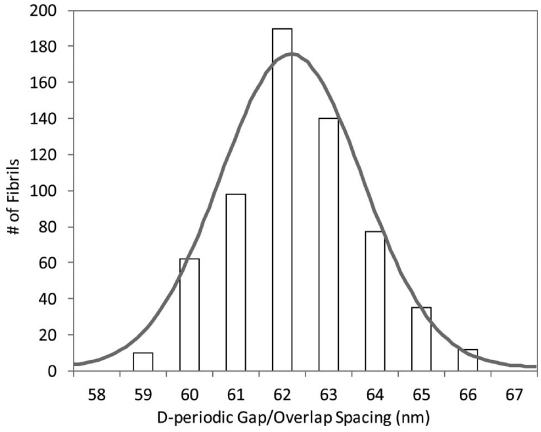

Figure 2. Typical *D*-spacing distribution from ovine dermis. Data were reproduced from AFM imaging and 2D FFT analysis of a sham control study in ref 33. The distribution is fitted to a Gaussian function shown as the curve.

Fourier transform (2D FFT) analysis.[31,32] Using this method, we have shown that a distribution of nanometer-scale *D*-spacings is present in a variety of type I collagen-based connective tissues, including bone, tooth, tendon, and dermis, from a number of species, including murine, ovine, and human.[31,33,34] An example of *D*-spacing distribution is shown in Figure 2.

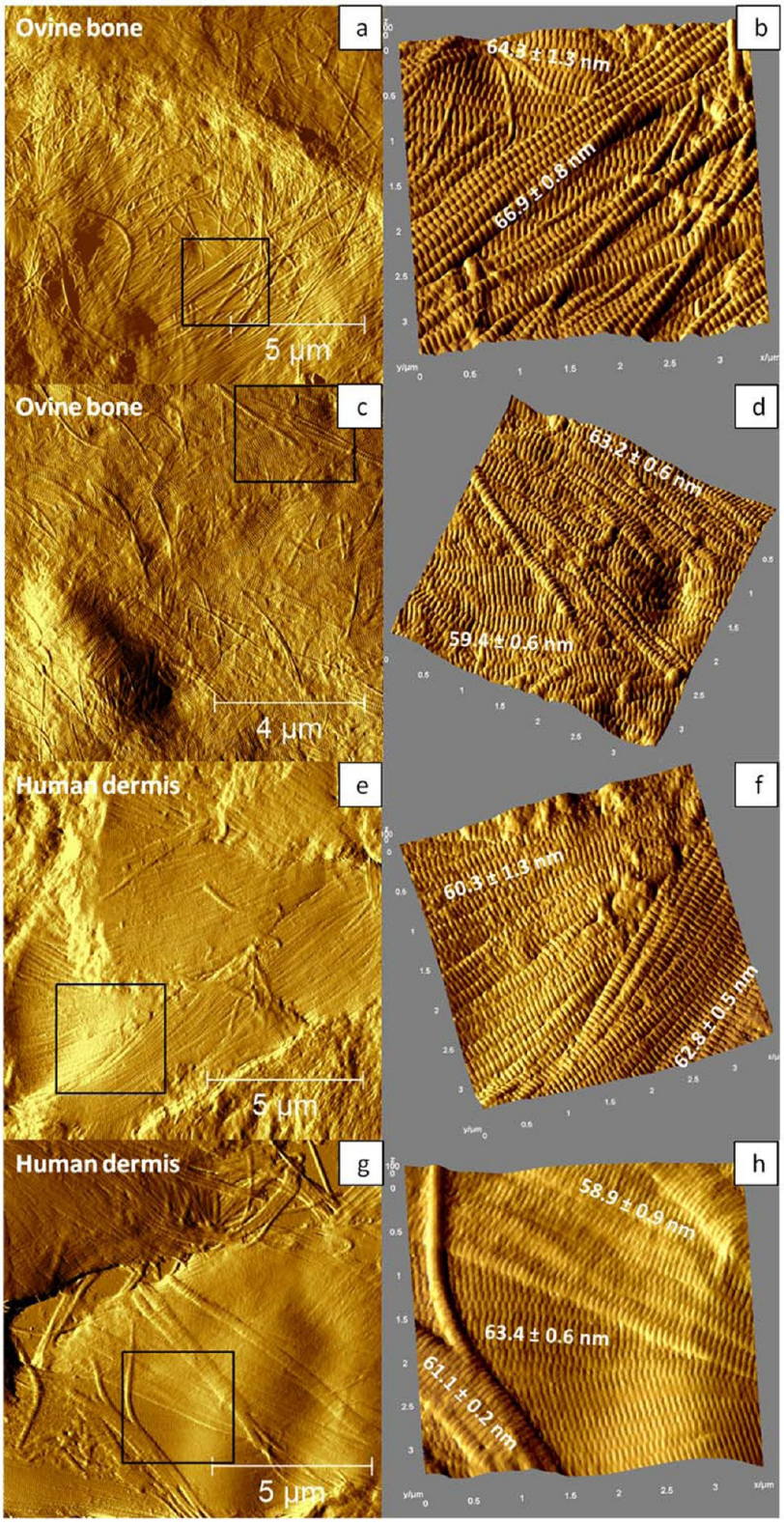

Figure 3. AFM images show the domains of fibril bundles and different *D*-spacings associated with them. (a−d) Exemplary images of ovine bone. (e−h) Exemplary images of human dermis. (b,d,f,h) Three dimensional topography plots of a 3.5 μm area marked by the black box in panel a, c, e and g, respectively. Panel b shows two bundles with 64.3 and 66.9 nm mean *D*-spacings; panel d shows two bundles with 63.2 and 59.4 nm *D*-spacing; panel f shows two bundles with 60.3 and 62.8 nm mean *D*-spacings; panel h shows three bundles with 58.9, 63.4 and 61.1 nm mean *D*-spacings.

The chemical and physical significance of the *distribution* of *D*-periodic axial spacing or "*D*-spacing" values, first characterized by electron microscopy in 1942,[35] has been largely overlooked for seven decades. Only a

TABLE 1. *D*-Spacing Mean, Average Angular Orientation, and Number of Fibrils of the Bundles Shown in Figure 3b,d,f,h[a]

	D-spacing (nm)			angular orientation (deg)			# of fibrils		
	B1	B2	B3	B1	B2	B3	B1	B2	B3
Figure 3b	64.3 (1.3)	66.9 (0.8)		−13.4 (4.6)	24.6 (7.7)		6	16	
Figure 3d	63.2 (0.6)	59.4 (0.6)		−15.9 (6.2)	22.1 (3.3)		8	8	
Figure 3f	60.3 (1.3)	62.8 (0.5)		10.7 (7.1)	38.9 (6.0)		9	10	
Figure 3h	58.9 (0.9)	63.4 (0.6)	61.1 (0.2)	−35.8 (10.0)	−3.0 (4.0)	−52.8 (1.8)	14	15	4

[a] The standard deviations are included in the parentheses. The angular orientation was measured with respect to the horizontal scan direction. B1−3 stands for bundles 1−3.

few publications have quantitatively described collagen *D*-spacing as a distribution of values to date.[35−38] The majority of publications have adopted the view, largely derived from X-ray scattering data,[39−41] that *D*-spacing is a single value of about 67 nm, and values deviating from this have generally been attributed to tissue-dependent differences[39,42] and/or artifacts of sample preparation methods such as dehydration.[36,40,43] However, we found that the *D*-spacing distributions were altered as a function of disease including estrogen deprivation induced osteopenia and *Osteogenesis Imperfecta*, suggesting the biological significance of the *D*-spacing distribution.[33,34,44]

In this study, the connection between the nanometer-scale collagen fibril *D*-spacing distribution and the micrometer-scale fibril bundle organization is explored. By comparing fibril *D*-spacings within a bundle and across different bundles, we wanted to test the two following hypotheses:

H1. The distribution of *D*-spacing arises from changes at the individual fibril level; that is, the fibril *D*-spacing is random with respect to the higher level bundle structure.

H2. The distribution of *D*-spacings arises from changes at the bundle level; that is, differences at the bundle level cause the full range of *D*-spacing values, whereas *D*-spacings within a bundle are similar.

We then discuss potential models of collagen fibril structure that describe the origin of the *D*-spacing morphology as well as the implications for currently proposed mechanisms of fibrillogenesis.

RESULTS

Collagen fibril bundles in healthy adult ovine bone and dermis, human dermis, and lamb tendon were imaged and analyzed. Typically, a fibril bundle was captured in one 3.5 μm × 3.5 μm AFM scan. In the case of ovine dermis and lamb tendon bundles, we collected images from multiple regions on a bundle (Figures 5 and 6). For all of the bundle data included in this study, the angular orientations of fibrils within a bundle varied by 10° or less in the *XY* plane; most fibrils in tendon bundles varied by 3° or less; most fibrils in dermis or bone bundles varied by 5° or less. The small differences of fibril angular orientation represent the laterally ordered organization in a fibril bundle, which serves as a primary criterion for selecting the bundles for quantitative analyses.

Different *D*-Spacings at Bundle Interfaces. Occasionally, two or more bundles were captured in one frame. Examples of these bundle interfaces are shown in Figure 3. Interestingly, even though the fibrils are spatially close to each other and captured by the same AFM tip in the same image, fibrils from different bundles exhibit distinctively different *D*-spacings; fibrils measured from the same bundle share similar *D*-spacing. Figure 3a,b illustrates a typical example of two lamella layers in ovine bone: in this instance, the underlying bundle has a mean *D*-spacing of 64.3 ± 1.3 nm, while the top bundle's *D*-spacing mean is 66.9 ± 0.8 nm. Another example of ovine bone is shown in Figure 3c,d, where the two bundles have *D*-spacing means of 63.2 ± 0.6 and 59.4 ± 0.6 nm. In addition to aligned fibril bundles, we observed additional interesting structures in bone. Examples of broom-like and interwoven fibril organizations are shown in Supporting Information Figure S1. Figure 3e shows a set of fibril bundles from human dermis, two of which were captured in Figure 3f, with *D*-spacings of 60.3 ± 1.3 and 62.8 ± 0.6 nm. Similarly, Figure 3g,h is from human dermis, and Figure 3h is a zoomed-in region of Figure 3g that captured three fibril bundles in one scan. The *D*-spacings are 58.9 ± 0.9, 63.4 ± 0.6, and 61.1 ± 0.2 nm. Average *D*-spacing and angular orientations of individual bundles are summarized in Table 1. In every case, differences among the bundles were statistically significant ($p < 0.001$).

Contribution of Bundle *D*-Spacing Variance to a 10 nm Width Distribution. To illustrate how bundle *D*-spacings contribute to tissue-scale *D*-spacing distributions, we color-coded the distribution histogram to show the contribution from different bundles (Figure 4). Taking ovine bone as an example, when plotted in a single histogram (Figure 4a,b), fibril bundle *D*-spacings range from 58 to 69 nm; however, within each fibril bundle, *D*-spacing generally spans 1−3 nm. Meanwhile, fibrils from different bundles exhibited independently variant *D*-spacings that contribute to the full ~10 nm distribution range in these tissues. The narrow intrabundle *D*-spacing distribution along with a wide tissue distribution was found for both ovine and human

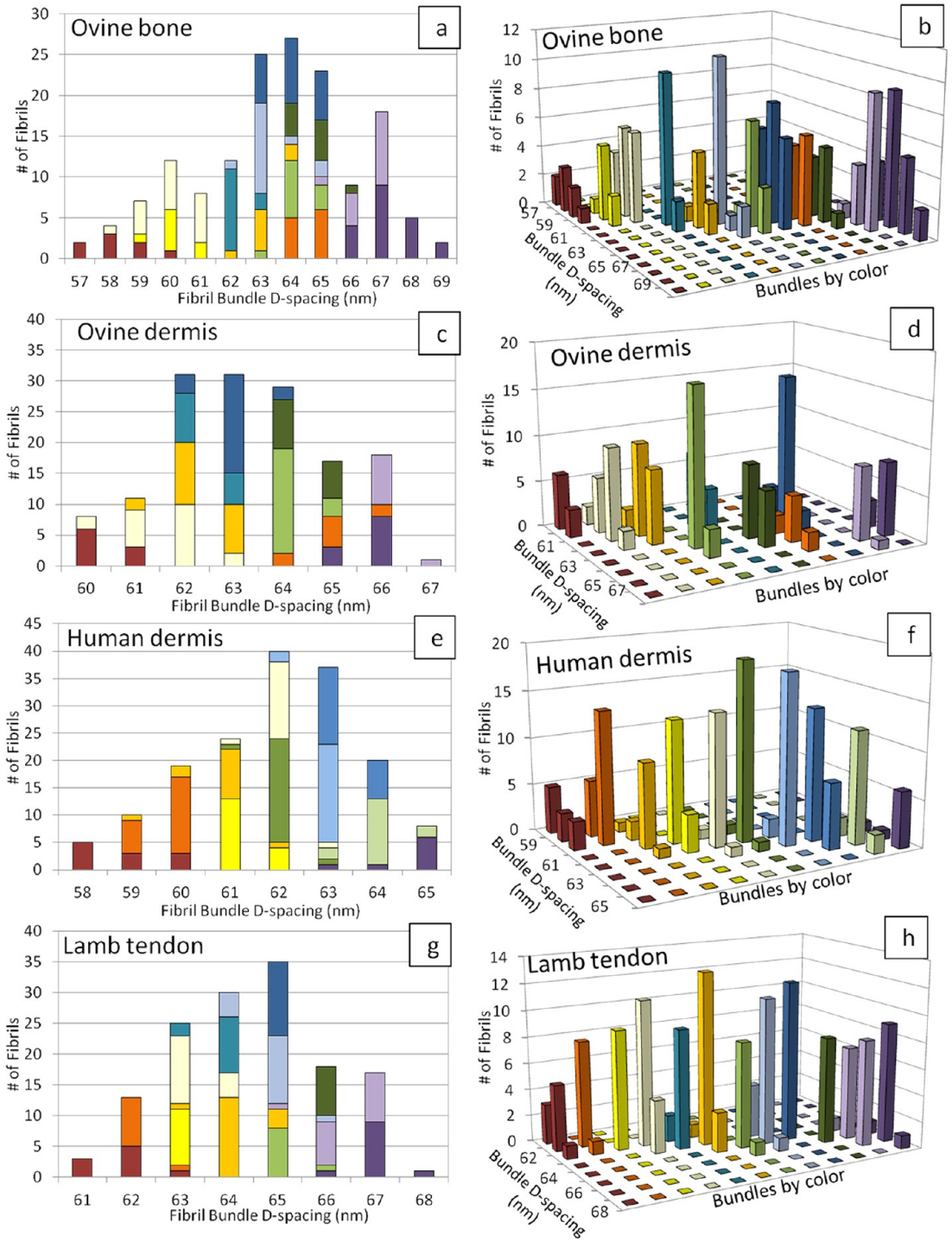

Figure 4. Collagen fibril *D*-spacing distribution arises from narrow bundle *D*-spacings in ovine bone, ovine dermis, human dermis and lamb tendon. *D*-spacing distributions plotted in histogram for (a) ovine bone, (c) ovine dermis, (e) human dermis, and (g) lamb tendon. Panels b, d, f, and h are 3D histograms of a, c, e, and g that show the narrow *D*-spacing values within a bundle. Each color bar indicates contributions of fibrils from one bundle, while different bundles are denoted by different colors.

tissues and for both mineralized (bone) and nonmineralized (dermis, tendon) tissue types (Figure 4).

When comparing fibril *D*-spacings from ovine and human dermis, the overall *D*-spacing averages of 63.0 and 62.5 nm, respectively, are not significantly different ($p = 0.24$). Upon employing a nested analysis of variance (mixed model ANOVA) to evaluate the contributions of the fibril, bundle, and animal variance to the range of *D*-spacing values, we found that bundle-to-bundle variance was the largest component, accounting for 78% of overall variance. The standard deviation (STD, symbol σ) between bundles is 1.3 nm, and the overall STD is 1.5 nm. The bundle STD is significantly different from 0 ($p < 0.0001$). In addition, bundle and fibril level

TABLE 2. Summary of Estimated Variance and Significance at the Levels of Animal, Bundle, and Fibril

test group	variance component	estimated variance σ^2 (STD: σ)	*P* value (compared to 0)
ovine dermis and human dermis (analysis 1)	animal - a_i	0.1 (0.4 nm)	0.2893
	bundle - b_{ij}	1.8 (1.3 nm)	<0.0001
	fibril - ε_{ijk}	0.4 (0.6 nm)	<0.0001
	overall variance	2.3 (1.5 nm)	
ovine bone, ovine dermis, and lamb tendon (analysis 2)	animal - a_i	0.4 (0.6 nm)	0.1594
	bundle - b_{ij}	2.5 (1.6 nm)	<0.0001
	fibril - ε_{ijk}	0.4 (0.6 nm)	<0.0001
	overall variance	3.3 (1.8 nm)	
ovine dermis[a] (analysis 3)	animal - a_i	0.5 (0.7 nm)	0.2198
	bundle - b_{ij}	1.5 (1.2 nm)	0.0021
	region - r_{ijl}	0.1 (0.4 nm)	0.1358
	fibril - ε_{ijkl}	0.4 (0.6 nm)	<0.0001
	overall variance	2.5 (1.6 nm)	
lamb tendon[a] (analysis 3)	animal - a_i	0.3 (0.5 nm)	0.3
	bundle - b_{ij}	1.3 (1.2 nm)	0.019
	region[b] - r_{ijl}	0.3—0.4 (0.6 nm)	0.0003
	fibril - ε_{ijkl}	0.2 (0.5 nm)	<0.0001
	overall variance	2.2 (1.5 nm)	

[a] See Supporting Information for the nested ANOVA model. [b] Estimated region-to-region variances are 0.4 for axial regions and 0.3 for perpendicular regions; the differences between them are not significant ($p = 0.78$, likelihood ratio χ^2 test).

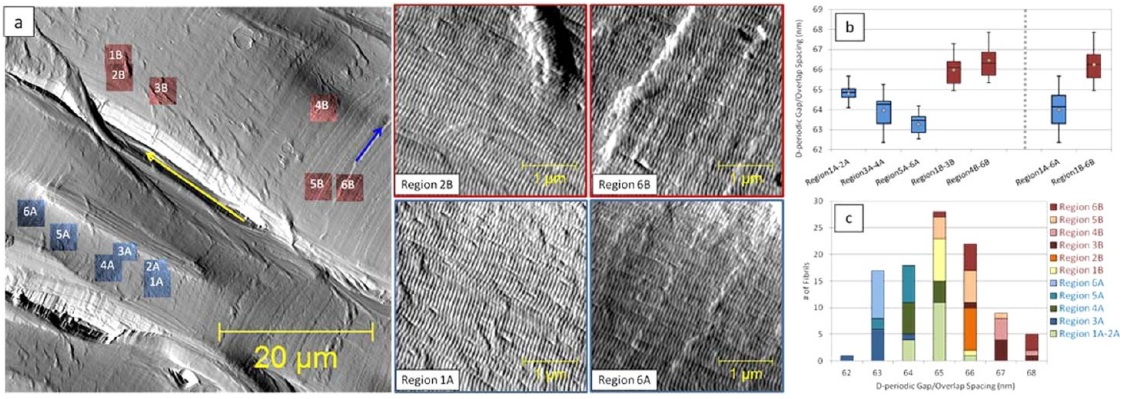

Figure 5. Persistence length of *D*-bundle in lamb tendon fascicle. Panel a is a 50 μm scan of two fascicles in lamb tendon, with the fascicle orientation marked by the yellow arrow. The diagonal lines (indicated by the blue arrow) are artifacts caused by a cryostat blade. Individual regions of 3.5 μm × 3.5 μm size were labeled by sequence and overlaid on the 50 μm scan. Regions 1A—6A are noted as fascicle A, while regions 1B—6B are noted as fascicle B. Panel b is the boxplot that reveals the interquartile, minimum, maximum, and mean of the *D*-periodic gap/overlap spacings measured from individual 3.5 μm scans. Panel c is the color-coded histogram of combined regions 1A—6A and 1B—6B.

variance are not different between ovine and human by likelihood ratio χ^2 test ($p > 0.999$ and $p = 0.86$, respectively). The data set exhibited a skewness on the low end of the distribution contributed by bundles with *D*-spacings as low as 58 nm. As a result, 4.8% of fibrils were found below $\mu_0 + \tau - 2\sigma$ and none above $\mu_0 + \tau + 2\sigma$.

The fibril *D*-spacing averages from ovine dermis, bone, and tendon, 62.9, 63.8, and 64.0 nm, respectively, are not significantly different from each other ($p = 0.12$). Similar to human/ovine dermis comparison, the nested analysis indicates the bundle level variance component differed from 0 ($p < 0.0001$), and it accounts for 76% of overall variance. The bundle level and overall STD are 1.6 and 1.8 nm, respectively. Interestingly, bundle variance differs substantially among the three tissues. For dermis, bone, and tendon, the estimated $\sigma^2_{\text{bundle(animal)}}$ values are 1.8, 3.8, and 1.4, respectively ($p = 0.074$ by likelihood ratio χ^2 test). Similarly, the fibril variance is also largest in bone and smallest in tendon. The estimated $\sigma^2_{\text{fibril(bundle(animal))}}$ values are 0.4, 0.5, and 0.2 for dermis, bone, and tendon, respectively ($p < 0.0001$). A summary of the statistical analysis is provided in Table 2. Additional detail of the nested analysis of variance mixed model ANOVA can be found in Supporting Information (Table S1).

Persistence Length of *D*-Spacings in Tendon Fascicles and Dermal Samples. Next, we investigated the persistence length of bundle *D*-spacings in lamb tendon fascicles and ovine dermis. Figure 5a shows two fascicles (A and B) of lamb tendon on the 50 μm scale. *D*-spacings were obtained from six 3.5 μm × 3.5 μm regions spaced over

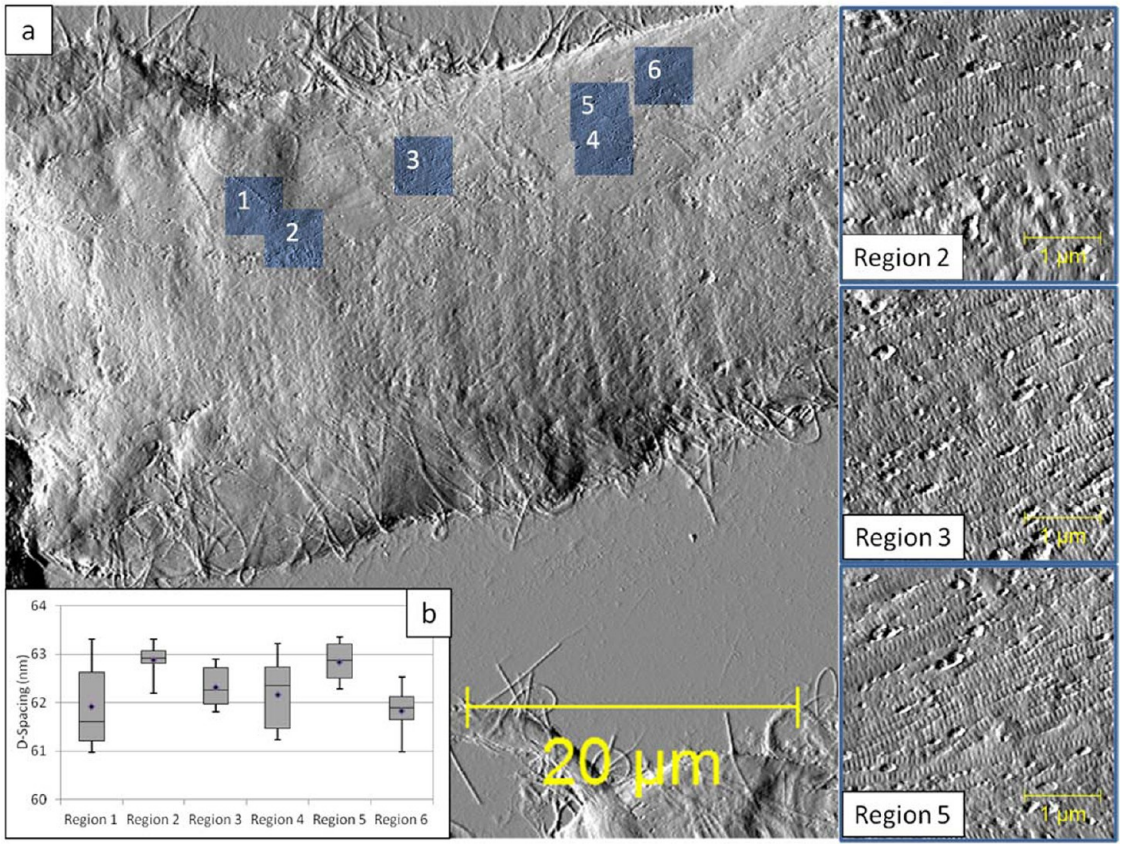

Figure 6. Persistence length of *D*-bundle in ovine dermis. Panel a is a 50 μm scan of a collagen fibril bundle in ovine dermis. Individual scans of 3.5 μm size were labeled by sequence and overlaid on the 50 μm scan (the missing numbers were 10 μm scans). Panel b is the boxplot that reveals the interquartile, minimum, maximum, and mean of the *D*-periodic gap/overlap spacings measured from individual 3.5 μm scans.

20 μm for fascicle A and 40 μm for fascicle B. Fascicles A and B have statistically different *D*-spacings ($p < 0.001$) of 64.0 $\pm$ 0.9 and 66.2 $\pm$ 0.9 nm, respectively. *D*-spacings have a 3.3 nm range in fascicle A and 2.9 nm in fascicle B. Within each fascicle, variations from region-to-region over a 50 μm scale are larger than variations within a 3.5 μm region. For example, region 1A has a mean *D*-spacing of 64.9 $\pm$ 0.3 nm, whereas region 6A has a mean *D*-spacing of 62.8 $\pm$ 0.3 nm. In another example, regions spaced over 40 μm length of a tendon fascicle give a 4.4 nm range of *D*-spacing values, with an overall mean of 64.1 $\pm$ 0.9 nm (Supporting Information, Figure S2). Nevertheless, the region-to-region variation is small compared to the full *D*-spacing width distribution. Nested model ANOVA estimates that region-to-region variance $\sigma^2_{\text{region(bundle(animal))}}$ in lamb tendon is 0.4, which is significantly lower than that of bundle-to-bundle variance, $\sigma^2_{\text{bundle(animal)}} = 1.3$ ($p = 0.0013$ by likelihood ratio χ^2 test). We also imaged perpendicular to the axial direction of one or more fascicles (Supporting Information, Figure S3). In this case, the range of *D*-spacings is 4 nm and the region-to-region variance $\sigma^2_{\text{region(bundle(animal))}}$ is 0.3. Finally, Figure 6 shows a fibril bundle of ovine dermis on the 50 μm scale. Six 3.5 μm $\times$ 3.5 μm regions spaced over 30 μm give a set of *D*-spacings for each region ranging from 61.8 $\pm$ 0.6 to 62.9 $\pm$ 0.4 nm with an overall average of 62.4 $\pm$ 0.7 nm. Nested model ANOVA estimates region-to-region variance $\sigma^2_{\text{region(bundle(animal))}}$ for ovine dermis is 0.1, significantly lower than bundle-to-bundle variance, $\sigma^2_{\text{bundle(animal)}} = 1.5$ ($p = 0.0102$ by likelihood ratio χ^2 test).

DISCUSSION

Origin of *D*-Spacing Distribution: *D*-Bundle. We have observed that collagen fibrils in a single bundle share similar *D*-spacings ($\pm$1 nm), and the full ~10 nm *D*-spacing distribution found in tissues[31,33,34,44] results from differences in bundle level *D*-spacing. This observation is supported by nested mixed model ANOVA analysis. When we evaluate the effect of tissue types, species, animals, bundles nested within animals, and fibrils nested within bundles and animals, the largest component of variance comes from the bundle-to-bundle variance. It accounts for over 76% of total variance, independent of tissue types (bone, dermis, and tendon) and species (ovine *vs* human). On the basis of these results, we propose a quantitative definition of a collagen bundle as a bundle of collagen fibrils characterized by identical *D*-spacing (with $\pm$1 nm STD),

and we will refer to fibril bundles with this property as *D*-bundles. Estimated from 107 *D*-bundles, STD within a *D*-bundle is 0.6 nm (see Table 2), which is within the error associated with AFM analysis;[31,32] therefore, the fibrils in each bundle have similar, if not identical, *D*-spacings. The bundle-to-bundle variations, as small as 1.3 nm STD in tendon and as large as 1.9 nm STD in bone, are the major components that give rise to the full distribution of 8−10 nm width and 1.5−2 nm STD, typically seen for tissue samples (an example is shown in Figure 2). These observations are consistent with hypothesis H2 and inconsistent with H1.

The bundle size, typically on the order of tens of micrometers, varies among tissues. As observed by AFM, the fibril bundle width in lamb tendon is 20 μm and larger; ovine and human dermis tend to have bundle width of a few micrometers in papillary dermis and 50 μm or larger in reticular dermis (similar observations in refs 38 and 45); fibril bundles in ovine cortical bone, in contrast to all other tissues used in this study, are less frequently observed and are usually of 1−5 μm in lateral size.

The question of persistence length of *D*-bundles is particularly interesting in tissues such as tendon, where fascicles can extend to millimeters in length. We evaluated the persistence length of *D*-bundles by taking *D*-spacing measurements across 40−50 μm axial and perpendicular directions of tendon fascicles. As shown in Figure 5 and Supporting Information Figures S2 and S3, *D*-spacings from regions of a tendon fascicle vary in a range of 4−5 nm. This range is between that of a *D*-bundle (1−3 nm range; 0.6 nm STD) and that of a tissue-scale *D*-spacing distribution (10 nm range; 1.5−2 nm STD). On the basis of nested ANOVA analysis, the region-to-region variance in the axial direction in lamb tendon is 0.4 (σ = 0.6 nm) and that of perpendicular direction is 0.3 (σ = 0.6 nm), which is significantly smaller than variance of different tendon bundles, 1.3 (σ = 1.2 nm). It suggests regions within a tendon fascicle vary to a lesser extent than different *D*-bundles in different fascicles and thus are more likely to be related to each other. In ovine dermis, the data in Figure 6 indicate that *D*-bundles can maintain a persistent *D*-spacing up to 30 μm in the axial direction, which is in agreement with the nested ANOVA analysis since the estimated region-to-region variance is 0.1 (σ = 0.4 nm).

Physical and/or Biochemical Origins of Bundle-Dependent *D*-Spacings. Knowing the physical and/or biochemical origins of tissue-scale *D*-spacing distribution and narrow *D*-bundle *D*-spacing range is imperative to our understanding of fibrillogenesis. Although this question remains to be answered, this section is devoted to discussing potential factors that could influence fibril *D*-spacing. First and foremost, it should be mentioned that biomineralization is not a determinant for the tissue-scale distribution of *D*-spacings since the 10 nm range of *D*-spacing and narrow *D*-spacing range in *D*-bundles are observed in both mineralized bone and nonmineralized dermis and tendon tissues.[31,34]

Mutations in the collagen composition can change the *D*-spacing. On the basis of a previous AFM study using an *Osteogenesis Imperfecta* (OI) mice model and molecular dynamics (MD) simulation, single substitution of glycine to cystein in collagen amino acid composition destabilizes the collagen triple helical structure,[46] and *D*-spacing distribution in the OI model showed significant shift from the control model.[44]

Some studies have shown *D*-spacing elongation as a function of strain.[47−49] However, elongation of *D*-spacing accounts only a small fraction of tissue level strain in the elastic deformation regime. Sasaki,[47] Puxkandl,[48] and Gupta *et al.*[49] have all shown in their studies that fibril strain tends to be on the order of 1−2 nm in tendon and bone. In our study, no external stress was applied to the tissues, and we observed ~10 nm range difference in bundle *D*-spacings. Therefore, it is very unlikely that strain alone is causing the bundle *D*-spacing differences.

Another hypothesis is that covalent cross-linking is responsible for *D*-bundle formation. It is possible that hydroxylysine sites are matched between adjacent fibrils during an enzymatic cross-linking process, resulting in overlapping gap zones and overlap zones.[50] In addition to enzymatic cross-linking, non-enzymatic glycation (NEG) such as cross-linking between collagen and sugar occurs with aging and diabetes.[51] However, we have found no effect of NEG on collagen fibril *D*-spacings using ovine bones treated with D-ribose *in vitro* (Supporting Information Figure S4). Similar results have been reported by Odetti and others.[37]

Other factors known to interact with collagen during formation and maturation include types V and XI collagen,[52,53] SLRPs such as decorin and lumican,[50,54,55] and fibronectin.[56−58] Knockout studies on collagen V or decorin have shown irregular fibril formation and in some cases early embryonic death,[55,59−61] suggesting indispensible roles that the minor collagen types and SLRPs play in regulating collagen fibril formation. However, little is known about whether these small proteins play a role in changing collagen fibril *D*-spacing.

In summary, the simplest form of the Hodge−Petruska model shown in Figure 1 does not address the variations of *D*-spacings reported here. In particular, these data indicate the need for collagen fibril growth and structural models to account for the collagen fibril *D*-spacings being organized at the hierarchical level of fibril bundles. As we understand more about the structural complexity of collagen and its dynamic interactions with other ECM components, it becomes increasingly important that we adopt a more sophisticated model of collagen fibril structure that also reflects *D*-spacing distribution. This model will allow us to better understand normal collagen hierarchy and

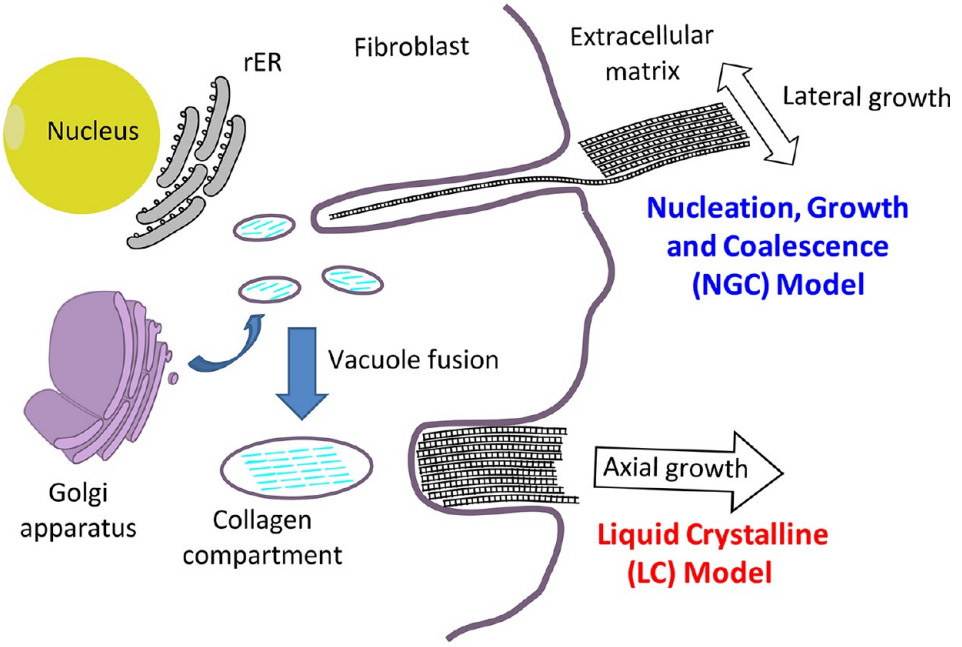

Figure 7. Scheme of NGC model and LC model. In the NGC model, the fibroblast forms ruffled protrusions or depressions called fibripositors. Collagen fibril nucleation and growth starts within fibripositors. Individual fibrils then coalesce into bundles when they are excreted into the ECM. In the LC model, collagen precursors prealign in secretary compartments or the ECM and form a bundle simultaneously.

changes in collagen structure induced by aging, diseases, and mechanical failures.

Collagen Fibril Bundle Formation in Fibrillogenesis Models. The mechanism of *D*-bundle formation is still an open question, and competing theories offer different views on the nucleation and growth of collagen fibrils.

Nucleation, Growth, and Coalescence (NGC) Model. EM studies by Birk's and Kadler's groups suggest a nucleation, growth, and coalescence model for the formation of collagen fibrils and fibril bundles (NGC model, Figure 7). In chick embryonic tendon, single or small groups of fibrils were found in membrane protrusions or depressions near fibroblast cell surfaces, which are called fibripositors.[62−64] On the basis of this observation, it is hypothesized that single collagen fibrils nucleate in these fibripositors and grow in the axial direction. Side-to-side fusion[26,30,62,65] as well as tip-to-tip fusion[55,66] of fibrils has been observed, which could explain the *D*-bundle formation. Our quantitative data on fibril *D*-spacing and their relationship to bundle structure place two interesting constraints on the NGC model. First, if *D*-spacing is determined by extracellular factors such as binding with proteoglycans and/or mechanical stress, then it is plausible that a bundle could share similar *D*-spacing if these factors exert uniform effect within a bundle. An alternative hypothesis is that *D*-spacing is determined at the fibripositor stage, which implies that bundle-dependent *D*-spacing is also cell-dependent. Although there is clear evidence indicating that intracellular information such as genetic coding can play a vital role in fibril *D*-spacing formation,[44] further experiments are required to clarify the relationship between collagen fibril *D*-spacing and the cells that produce collagen.

Liquid-Crystalline (LC) Model. Driven by the observation of liquid-crystalline properties in type I collagen[67−69] *in vitro*, Giraud-Guille and others have proposed that collagen precursors (procollagen or tropocollagen) are prealigned in concentrated local environments, which aids in the alignment, undulations, and twists in the packing of collagen fibrils (LC model, Figure 7).[70] It is also interesting to note that the plywood structure of human compact bone osteons is analogous to the organization of cholesteric liquid crystals, as the direction of fibrils rotates by a constant angle from one lamallar layer to the next.[24,29,68] This model provides a simple physical explanation for the collagen structural organization in collective tissues and offers the intriguing possibility that *D*-bundle spacing is synchronized by liquid-crystalline alignment. Although aspects of this model are compelling, the liquid crystallinity of collagen has not been demonstrated directly *in vivo*.

CONCLUSION

In conclusion, we observed a narrow distribution of *D*-spacings within *D*-bundles (±1 nm). In addition, large variations in *D*-spacings among different bundles contribute to the full distribution (10 nm range) at the tissue scale in bone, dermis, and tendon. The measurements and statistical analysis support the hypothesis that differences at the bundle level cause the full range of *D*-spacing values, whereas *D*-spacings within a bundle are similar (H2) and are inconsistent with fibril *D*-spacing being random with respect to the higher

level bundle structure (H1). The formation of *D*-bundles has important implications in terms of how collagen fibrils are assembled; however, the mechanisms of *D*-bundle formation and *D*-spacing variations are poorly understood. Mechanistic pathways for both the NGC and LC models can be proposed that are consistent with the data presented here for the relationship between fibril *D*-spacing and bundle structure. Future research efforts are needed to answer many questions raised by these studies including the following: How are cells and/or extracellular proteins involved in forming collagen fibril bundles? What contributes to a heterogeneous *D*-spacing distribution? Is the tight distribution of *D*-spacings within a *D*-bundle disrupted by disease? Do *D*-bundles with different *D*-spacings play varying roles under mechanical stresses? We are pursuing a number of these challenging questions, and we hope that these new quantitative observations regarding type I collagen structure can be employed by the broader scientific community to promote a better understanding of collagen fibrillogenesis and ultimately how collagenous tissues are established and maintained.

EXPERIMENTAL METHOD

Animals. Ovine bone and dermis specimens were collected from sham-operated Columbia-Rambouillet ovine, as previously described.[33] Bone specimens were acquired from the mid-diaphysis of the left radius, while dermis specimens were harvested from the dorsal midline, in the thoracolumbar region. Procurement of human skin samples was approved the University of Michigan Institutional Review Board and conducted according to the Declaration of Helsinki principles. All subjects provided written informed consent. Full-thickness human skin biopsies were taken from sun-protected buttock skin from human donors ranging in age from 20 to 40 years old. Lamb tendons were from 6 month old rambouillet-dorset ovine, provided by a local butcher. Ovine bone data were collected from 15 animals; ovine dermis data were collected from 4 animals; human dermis data were collected from 6 donors; lamb tendon data were collected from 4 animals. We analyzed 32 bundles in ovine bone, 26 in ovine dermis, 32 in human dermis, and 17 in lamb tendon for a total of 107 bundles and 1710 fibrils.

Cryostat Sectioning of Dermis and Tendon. Combined tissue sectioning and AFM analysis was highlighted in Graham's recent report.[71] First, skin biopsies were embedded in Tissue-Tek optimal cutting temperature (OCT) solution (Sakura Finetek Inc., Torrance, CA, USA) and frozen at −20 °C. Ten micrometer thick thin sections of dermis were obtained using Microm HM550 cryostat (Thermo Scientific Inc., Walldorf, Germany) and transferred onto glass slides. Due to the random meshwork nature of dermis collagen bundles, sections parallel to the skin surface and perpendicular to the skin surface (cross section) are both suited for AFM imaging. The dermal sections were rinsed with ultrapure water for 5 min and kept at −20 °C prior to the AFM study. Tendon specimens were sectioned in a similar manner, and the cutting plane was set to be parallel with the long axis of tendon. No artificial stretching was imposed on tissue samples during sample preparation.

Polishing and Demineralization of Bone. Ovine bones were mounted to a steel disk using cyanoacrylate glue, and a flat surface was polished as described previously.[33] The bones were demineralized using 0.5 M EDTA at a pH of 8.0 for 1 h with 5 min sonication at every 20 min interval. The bones were then vigorously rinsed with ultrapure water and preserved at 4 °C before AFM study.

Atomic Force Microscopy (AFM) Imaging and Analysis. All imaging was carried out in air-dry condition using a PicoPlus 5500 AFM (Agilent); dermis and tendon specimens were imaged in contact mode using SNL-10 AFM probes (Bruker AFM probes, nominal tip radius 2 nm, force constant 0.25 N/m). Ovine bones were imaged using tapping mode with VistaProbes T300R probes (NanoScience, AZ; nominal radius 10 nm, force constant 40 N/m, resonance frequency 300 kHz). Line scan rates were set at 2 Hz or lower at 512 lines per frame. Random locations on tissue samples were imaged by AFM in search of fibril bundles. Image analysis and measurements were performed using SPIP software (V5.0.8, Image Metrology; Horsholm, Denmark). Collagen fibril *D*-spacings were measured using 2D fast Fourier transform (FFT) toolkit of SPIP software; detailed description and validation can be found in previous studies.[31,33]

One concern associated with AFM imaging is the effect of thermal drift and tip convolution which may differ from scan to scan. We have carefully examined the effect of thermal drifting and ruled out the possibility of thermal drifting causing an artificial *D*-spacing distribution.[32] Furthermore, finding two or more fibril bundles with different *D*-spacings in single AFM scans (Figure 3) rules out the concern that the differences in *D*-spacings may be caused by using different AFM tips or scanning on different days. All fibril bundle *D*-spacings were measured within individual 50 μm × 50 μm area. The limited AFM scan size may underestimate lateral bundle size and persistence length. In addition, due to the cylindrical geometry of bone lamellae, polishing and imaging on a flat surface may cause underestimation in the bundle size and length of fibril bundles in bone tissues.

Statistical Analysis. Mean *D*-spacings (±standard deviation) from individual bundles were tested using one way ANOVA.

A nested analysis of variance was employed (mixed model ANOVA[72]) to determine the hierarchical level of the sources of variance in the overall *D*-spacing distribution (eqs a−e). Arranged by their hierarchical order, fibrils were nested within bundles and bundles were nested within animals.

$$Y_{ijk} = \mu_0 + \tau + a_i + b_{ij} + \varepsilon_{ijk} \quad \text{(a)}$$

$$\text{var}(a_i) = \sigma^2_{\text{animal}} \quad \text{(b)}$$

$$\text{var}(b_{ij}) = \sigma^2_{\text{bundle(animal)}} \quad \text{(c)}$$

$$\text{var}(\varepsilon_{ijk}) = \sigma^2_{\text{fibril(bundle(animal))}} \quad \text{(d)}$$

$$\text{totalvariance} = \sigma^2_{\text{animal}} + \sigma^2_{\text{bundle(animal)}} + \sigma^2_{\text{fibril(bundle(animal))}} \quad \text{(e)}$$

where μ_0 is *D*-spacing mean; τ is fixed effect (described in the analyses below); a_i is random effect of *i*th animal; b_{ij} is random effect of *j*th bundle nested within *i*th animal; ε_{ijk} is random effect of *k*th fibril nested in *j*th bundle and in *i*th animal.

Two sets of mixed model ANOVA analyses were performed based on the model above:

Analysis 1: Comparison of two different species: ovine dermis (4 animals, 26 bundles, and 340 fibrils) and human dermis (6 humans, 32 bundles, and 479 fibrils); in this case, the fixed effect τ is the animal type.

Analysis 2: Comparison of three different tissue types in ovine: ovine bone (15 animals, 32 bundles, 340 fibrils), ovine dermis (4 animals, 26 bundles, and 340 fibrils), and lamb tendon (4 animals, 17 bundles, 198 fibrils); in this case, the fixed effect τ is the tissue type.

Within each nested analysis, differences between *D*-spacing averages, components of variance, and their significance were examined. It should be noted that only one 3.5 μm × 3.5 μm region per bundle is used in these two analyses.

In 1 of the 26 bundles in ovine dermis (Figure 6) and 4 of 17 bundles in lamb tendon (Figure 5 and Supporting Information Figure S2), we investigated multiple regions along the axial direction of one bundle or fascicle (over ~20−40 μm distance) to assess the axial persistence length of these bundles. We examined regions perpendicular to one fascicle (over ~40 μm distance) in lamb tendon (Supporting Information Figure S3). We employed another nested model (see Supporting Information, S. Eqs a−f) to include the variance component of regions.

Analysis 3: Estimate the region-to-region variance, and how it compares to bundle-to-bundle variance: ovine dermis (4 animals, 26 bundles, 31 locations, and 376 fibrils); lamb tendon (4 animals, 17 bundles, 49 locations, and 515 fibrils).

Conflict of Interest: The authors declare no competing financial interest.

Acknowledgment. We thank Electron Microscopy & Image Analysis Laboratory at U of M for the technical assistance on cryostat sectioning. The procurement of human skin samples was supported by NIH Grant AG025186.

Supporting Information Available: Diverse fibril organization in bone (Figure S1); longitudinal and lateral persistence length of *D*-spacings in lamb tendon bundles (Figure S2 and S3); experimental data of *in vitro* non-enzymatic glycation treatment (Figure S4). Supporting equations S. Eq a−f: nested ANOVA model for bundle persistence length assessment. Table S1: Summary of nested ANOVA test results. This material is available free of charge *via* the Internet at http://pubs.acs.org.

REFERENCES AND NOTES

1. Naylor, E. C.; Watson, R. E. B.; Sherratt, M. J. Molecular Aspects of Skin Ageing. *Maturitas* **2011**, *69*, 249–256.
2. Verzijl, N.; DeGroot, J.; Thorpe, S. R.; Bank, R. A.; Shaw, J. N.; Lyons, T. J.; Bijlsma, J. W. J.; Lafeber, F. P. J. G.; Baynes, J. W.; TeKoppele, J. M. Effect of Collagen Turnover on the Accumulation of Advanced Glycation End Products. *J. Biol. Chem.* **2000**, *275*, 39027–39031.
3. Orgel, J. P. R. O.; Irving, T. C.; Miller, A.; Wess, T. J. Microfibrillar Structure of Type I Collagen *in Situ*. *Proc. Natl. Acad. Sci. U.S.A.* **2006**, *103*, 9001–9005.
4. Sasaki, N.; Nakayama, Y.; Yoshikawa, M.; Enyo, A. Stress Relaxation Function of Bone and Bone Collagen. *J. Biomech.* **1993**, *26*, 1369–1376.
5. Sivakumar, P.; Czirok, A.; Rongish, B. J.; Divakara, V. P.; Wang, Y. P.; Dallas, S. L. New Insights into Extracellular Matrix Assembly and Reorganization from Dynamic Imaging of Extracellular Matrix Proteins in Living Osteoblasts. *J. Cell Sci.* **2006**, *119*, 1350–1360.
6. Dallas, S. L.; Chen, Q.; Sivakumar, P. Dynamics of Assembly and Reorganization of Extracellular Matrix Proteins. In *Current Topics in Developmental Biology*; Gerald, P. S., Ed.; Academic Press: New York, 2006; Vol. 75, pp 1−24.
7. Fratzl, P. SpringerLink. *Collagen Structure and Mechanics*; Springer Science+Business Media, LLC: Boston, MA, 2008.
8. Miller, A.; Wray, J. S. Molecular Packing in Collagen. *Nature* **1971**, *230*, 437–439.
9. Hulmes, D. J. S.; Miller, A. Quasi-Hexagonal Molecular Packing in Collagen Fibrils. *Nature* **1979**, *282*, 878–880.
10. Fraser, R. D. B.; MacRae, T. P.; Miller, A.; Suzuki, E. Molecular Conformation and Packing in Collagen Fibrils. *J. Mol. Biol.* **1983**, *167*, 497–521.
11. Fraser, R. D. B.; MacRae, T. P.; Miller, A. Molecular Packing in Type I Collagen Fibrils. *J. Mol. Biol.* **1987**, *193*, 115–125.
12. Trus, B. L.; Piez, K. A. Compressed Microfibril Models of the Native Collagen Fibril. *Nature* **1980**, *286*, 300–301.
13. Traub, W.; Piez, K. A. The Chemistry and Structure of Collagen. *Adv. Protein Chem.* **1971**, *25*, 243–352.
14. Piez, K. A.; Trus, B. L. A New Model for Packing of Type-I Collagen Molecules in the Native Fibril. *Biosci. Rep.* **1981**, *1*, 801–810.
15. Brodsky, B.; Eikenberry, E. F. Characterization of Fibrous Forms of Collagen. In *Methods of Enzymology*; Academic Press: New York, 1982; Vol. 82, pp 127−174.
16. Hulmes, D. J. S.; Wess, T. J.; Prockop, D. J.; Fratzl, P. Radial Packing, Order, and Disorder in Collagen Fibrils. *Biophys. J.* **1995**, *68*, 1661–1670.
17. Hodge, A. J.; Petruska, J. A. *Recent Studies with the Electron Microscope on Ordered Aggregates of the Tropocollagen Molecule*; Academic Press: New York, 1963; pp 289−300.
18. Knott, L.; Bailey, A. J. Collagen Cross-Links in Mineralizing Tissues: A Review of Their Chemistry, Function, and Clinical Relevance. *Bone* **1998**, *22*, 181–187.
19. Lavker, R. M.; Zheng, P.; Dong, G. Aged Skin: A Study by Light, Transmission Electron, and Scanning Electron Microscopy. *J. Invest. Dermatol.* **1987**, *88*, 44s–51s.
20. Goldsmith, L. A. *Physiology, Biochemistry, and Molecular Biology of the Skin*; Oxford University Press: New York, 1991; p 2v (xxii, 1529 pp).
21. Kannus, P. Structure of the Tendon Connective Tissue. *Scand. J. Med. Sci. Sports* **2000**, *10*, 312–320.
22. Provenzano, P. P.; Vanderby, R., Jr. Collagen Fibril Morphology and Organization: Implications for Force Transmission in Ligament and Tendon. *Matrix Biol.* **2006**, *25*, 71–84.
23. Weiner, S.; Arad, T.; Sabanay, I.; Traub, W. Rotated Plywood Structure of Primary Lamellar Bone in the Rat: Orientations of the Collagen Fibril Arrays. *Bone* **1997**, *20*, 509–514.
24. Giraud-Guille, M. M. Twisted Plywood Architecture of Collagen Fibrils in Human Compact Bone Osteons. *Calcif. Tissue Int.* **1988**, *42*, 167–180.
25. Weiner, S.; Wagner, H. D. The Material Bone: Structure-Mechanical Function Relations. *Annu. Rev. Mater. Sci.* **1998**, *28*, 271–298.
26. Birk, D. E.; Trelstad, R. L. Extracellular Compartments in Tendon Morphogenesis: Collagen Fibril, Bundle, and Macroaggregate Formation. *J. Cell Biol.* **1986**, *103*, 231–240.
27. Birk, D. E.; Trelstad, R. L. Extracellular Compartments in Matrix Morphogenesis: Collagen Fibril, Bundle, and Lamellar Formation by Corneal Fibroblasts. *J. Cell Biol.* **1984**, *99*, 2024–2033.
28. Birk, D. E.; Southern, J. F.; Zycband, E. I.; Fallon, J. T.; Trelstad, R. L. Collagen Fibril Bundles: A Branching Assembly Unit in Tendon Morphogenesis. *Development* **1989**, *107*, 437–443.
29. Bromage, T. G.; Goldman, H. M.; McFarlin, S. C.; Warshaw, J.; Boyde, A.; Riggs, C. M. Circularly Polarized Light Standards for Investigations of Collagen Fiber Orientation in Bone. *Anat. Rec., Part B* **2003**, *274*, 157–168.
30. Yurchenco, P. D.; Birk, D. E.; Mecham, R. P. *Extracellular Matrix Assembly and Structure*; Academic Press: San Diego, CA, 1994; p xi, 468 pp.
31. Wallace, J. M.; Chen, Q.; Fang, M.; Erickson, B.; Orr, B. G.; Banaszak Holl, M. M. Type I Collagen Exists as a Distribution of Nanoscale Morphologies in Teeth, Bones, and Tendons. *Langmuir* **2010**, *26*, 7349–7354.
32. Erickson, B.; Fang, M.; Wallace, J. M.; Orr, B. G.; Les, C. M.; Banaszak Holl, M. M. Nanoscale Structure of Type I Collagen Fibrils: Quantitative Measurement of *D*-Spacing. *Biotechnol. J.* **2012**, DOI: 10.1002/biot.201200174.
33. Wallace, J. M.; Erickson, B.; Les, C. M.; Orr, B. G.; Banaszak Holl, M. M. Distribution of Type I Collagen Morphologies in Bone: Relation to Estrogen Depletion. *Bone* **2010**, *46*, 1349–1354.
34. Fang, M.; Liroff, K. G.; Turner, A. S.; Les, C. M.; Orr, B. G.; Banaszak Holl, M. M. Estrogen Depletion Results in Nanoscale Morphology Changes in Dermal Collagen. *J. Invest. Dermatol.* **2012**, *132*, 1791–1797.
35. Schmitt, F. O.; Hall, C. E.; Jakus, M. A. Electron Microscope Investigations of the Structure of Collagen. *J. Cell. Comp. Physiol.* **1942**, *20*, 11–33.
36. Habelitz, S.; Balooch, M.; Marshall, S. J.; Balooch, G.; Marshall, G. W., Jr. *In Situ* Atomic Force Microscopy of Partially Demineralized Human Dentin Collagen Fibrils. *J. Struct. Biol.* **2002**, *138*, 227–236.
37. Odetti, P.; Aragno, I.; Rolandi, R.; Garibaldi, S.; Valentini, S.; Cosso, L.; Traverso, N.; Cottalasso, D.; Pronzato, M. A.; Marinari, U. M. Scanning Force Microscopy Reveals Structural Alterations in Diabetic Rat Collagen Fibrils: Role of Protein Glycation. *Diabetes/Metab. Res. Rev.* **2000**, *16*, 74–81.

38. Gross, J.; Schmitt, F. O. The Structure of Human Skin Collagen as Studied with the Electron Microscope. *J. Exp. Med.* **1948**, *88*, 555–568.
39. Brodsky, B.; Eikenberry, E. F.; Cassidy, K. An Unusual Collagen Periodicity in Skin. *Biochim. Biophys. Acta* **1980**, *621*, 162–166.
40. Bear, R. S. X-ray Diffraction Studies on Protein Fibers. I. The Large Fiber-Axis Period of Collagen. *J. Am. Chem. Soc.* **1944**, *66*, 1297–1305.
41. Price, R. I.; Lees, S.; Kirschner, D. A. X-ray Diffraction Analysis of Tendon Collagen at Ambient and Cryogenic Temperatures: Role of Hydration. *Int. J. Biol. Macromol.* **1997**, *20*, 23–33.
42. Stinson, R. H.; Sweeny, P. R. Skin Collagen Has an Unusual *D*-Spacing. *Biochim. Biophys. Acta* **1980**, *621*, 158–161.
43. Eikenberry, E. F.; Brodsky, B. B.; Craig, A. S.; Parry, D. A. D. Collagen Fibril Morphology in Developing Chick Metatarsal Tendon: 2. Electron Microscope Studies. *Int. J. Biol. Macromol.* **1982**, *4*, 393–398.
44. Wallace, J. M.; Orr, B. G.; Marini, J. C.; Banaszak Holl, M. M. B. Nanoscale Morphology of Type I Collagen Is Altered in the Brtl Mouse Model of Osteogenesis Imperfecta. *J. Struct. Biol.* **2011**, *173*, 146–152.
45. Verhaegen, P. D. H. M.; Van Marle, J.; Kuehne, A.; Schouten, H. J.; Gaffney, E. A.; Maini, P. K.; Middelkoop, E.; van Zuijlen, P. P. M. Collagen Bundle Morphometry in Skin and Scar Tissue: A Novel Distance Mapping Method Provides Superior Measurements Compared to Fourier Analysis. *J. Microsc.* **2012**, *245*, 82–89.
46. Lee, K. H.; Kuczera, K.; Banaszak Holl, M. M. The Severity of Osteogenesis Imperfecta: A Comparison to the Relative Free Energy Differences of Collagen Model Peptides. *Biopolymers* **2011**, *95*, 182–193.
47. Sasaki, N.; Shukunami, N.; Matsushima, N.; Izumi, Y. Time-Resolved X-ray Diffraction from Tendon Collagen during Creep Using Synchrotron Radiation. *J. Biomech.* **1999**, *32*, 285–292.
48. Puxkandl, R.; Zizak, I.; Paris, O.; Keckes, J.; Tesch, W.; Bernstorff, S.; Purslow, P.; Fratzl, P. Viscoelastic Properties of Collagen: Synchrotron Radiation Investigations and Structural Model. *Philos. Trans. R. Soc., B* **2002**, *357*, 191–197.
49. Gupta, H. S.; Zioupos, P. Fracture of Bone Tissue: The 'Hows' and the 'Whys'. *Med. Eng. Phys.* **2008**, *30*, 1209–1226.
50. Orgel, J. P. R. O.; San Antonio, J. D.; Antipova, O. Molecular and Structural Mapping of Collagen Fibril Interactions. *Connect. Tissue Res.* **2011**, *52*, 2–17.
51. Vashishth, D.; Gibson, G. J.; Khoury, J. I.; Schaffler, M. B.; Kimura, J.; Fyhrie, D. P. Influence of Nonenzymatic Glycation on Biomechanical Properties of Cortical Bone. *Bone* **2001**, *28*, 195–201.
52. Wenstrup, R. J.; Florer, J. B.; Brunskill, E. W.; Bell, S. M.; Chervoneva, I.; Birk, D. E. Type V Collagen Controls the Initiation of Collagen Fibril Assembly. *J. Biol. Chem.* **2004**, *279*, 53331–53337.
53. Wenstrup, R. J.; Smith, S. M.; Florer, J. B.; Zhang, G.; Beason, D. P.; Seegmiller, R. E.; Soslowsky, L. J.; Birk, D. E. Regulation of Collagen Fibril Nucleation and Initial Fibril Assembly Involves Coordinate Interactions with Collagens V and XI in Developing Tendon. *J. Biol. Chem.* **2011**, *286*, 20455–20465.
54. Weber, I. T.; Harrison, R. W.; Iozzo, R. V. Model Structure of Decorin and Implications for Collagen Fibrillogenesis. *J. Biol. Chem.* **1996**, *271*, 31767–31770.
55. Graham, H. K.; Holmes, D. F.; Watson, R. B.; Kadler, K. E. Identification of Collagen Fibril Fusion during Vertebrate Tendon Morphogenesis. The Process Relies on Unipolar Fibrils and Is Regulated by Collagen–Proteoglycan Interaction. *J. Mol. Biol.* **2000**, *295*, 891–902.
56. Kadler, K. E.; Hill, A.; Canty-Laird, E. G. Collagen Fibrillogenesis: Fibronectin, Integrins, and Minor Collagens as Organizers and Nucleators. *Curr. Opin. Cell Biol.* **2008**, *20*, 495–501.
57. Singh, P.; Carraher, C.; Schwarzbauer, J. E. Assembly of Fibronectin Extracellular Matrix. In *Annual Review of Cell and Developmental Biology*; Schekman, R.; Goldstein, L.; Lehmann, R., Eds.; Kluwer: Dordrecht, The Netherlands, 2010; Vol. 26, pp 397–419.
58. Shi, F.; Harman, J.; Fujiwara, K.; Sottile, J. Collagen I Matrix Turnover Is Regulated by Fibronectin Polymerization. *Am. J. Physiol.* **2010**, *298*, C1265–C1275.
59. Reed, C. C.; Iozzo, R. V. The Role of Decorin in Collagen Fibrillogenesis and Skin Homeostasis. *Glycoconjugate J.* **2002**, *19*, 249–255.
60. Danielson, K. G.; Baribault, H.; Holmes, D. F.; Graham, H.; Kadler, K. E.; Iozzo, R. V. Targeted Disruption of Decorin Leads to Abnormal Collagen Fibril Morphology and Skin Fragility. *J. Cell Biol.* **1997**, *136*, 729–743.
61. Zhang, G.; Ezura, Y.; Chervoneva, I.; Robinson, P. S.; Beason, D. P.; Carine, E. T.; Soslowsky, L. J.; Iozzo, R. V.; Birk, D. E. Decorin Regulates Assembly of Collagen Fibrils and Acquisition of Biomechanical Properties during Tendon Development. *J. Cell. Biochem.* **2006**, *98*, 1436–1449.
62. Canty, E. G.; Kadler, K. E. Procollagen Trafficking, Processing and Fibrillogenesis. *J. Cell Sci.* **2005**, *118*, 1341–1353.
63. Canty, E. G.; Lu, Y.; Meadows, R. S.; Shaw, M. K.; Holmes, D. F.; Kadler, K. E. Coalignment of Plasma Membrane Channels and Protrusions (Fibripositors) Specifies the Parallelism of Tendon. *J. Cell Biol.* **2004**, *165*, 553–563.
64. Trelstad, R. L.; Hayashi, K. Tendon Collagen Fibrillogenesis: Intracellular Subassemblies and Cell Surface Changes Associated with Fibril Growth. *Dev. Biol.* **1979**, *71*, 228–242.
65. Hay, E. D. *Cell Biology of Extracellular Matrix*l Plenum Press: New York, 1991; p xvii, 468 pp.
66. Kadler, K. E.; Holmes, D. F.; Trotter, J. A.; Chapman, J. A. Collagen Fibril Formation. *Biochem. J.* **1996**, *316*, 1–11.
67. Giraud-Guille, M. M. Liquid Crystallinity in Condensed Type I Collagen Solutions. A Clue to the Packing of Collagen in Extracellular Matrices. *J. Mol. Biol.* **1992**, *224*, 861–873.
68. Giraud-Guille, M. M.; Mosser, G.; Belamie, E. Liquid Crystallinity in Collagen Systems *in Vitro* and *in Vivo*. *Curr. Opin. Colloid Interface Sci.* **2008**, *13*, 303–313.
69. Gobeaux, F.; Mosser, G.; Anglo, A.; Panine, P.; Davidson, P.; Giraud-Guille, M. M.; Belamie, E. Fibrillogenesis in Dense Collagen Solutions: A Physicochemical Study. *J. Mol. Biol.* **2008**, *376*, 1509–1522.
70. Giraud-Guille, M. M.; Belamie, E.; Mosser, G.; Helary, C.; Gobeaux, F.; Vigier, S. Liquid Crystalline Properties of Type I Collagen: Perspectives in Tissue Morphogenesis. *CR Chimie* **2008**, *11*, 245–252.
71. Graham, H. K.; Hodson, N. W.; Hoyland, J. A.; Millward-Sadler, S. J.; Garrod, D.; Scothern, A.; Griffiths, C. E. M.; Watson, R. E. B.; Cox, T. R.; Erler, J. T.; *et al.* Tissue Section AFM: *In Situ* Ultrastructural Imaging of Native Biomolecules. *Matrix Biol.* **2010**, *29*, 254–260.
72. West, B. T.; Welch, K. B.; Galecki, A. T.; NetLibrary, I. *Linear Mixed Models: A Practical Guide Using Statistical Software*; Chapman & Hall/CRC: Boca Raton, FL, 2007; p cm.